Demonstration of the Casimir Force between Ferromagnetic Surfaces of a Ni-Coated Sphere and a Ni-Coated Plate

A. A. Banishev,[1] G. L. Klimchitskaya,[2] V. M. Mostepanenko,[2] and U. Mohideen[1]

[1]*Department of Physics and Astronomy, University of California, Riverside, California 92521, USA*
[2]*Central Astronomical Observatory at Pulkovo of the Russian Academy of Sciences, St. Petersburg 196140, Russia*
(Received 31 August 2012; published 25 March 2013)

We demonstrate the Casimir interaction between two ferromagnetic boundary surfaces using the dynamic atomic force microscope. The experimental data are found to be in excellent agreement with the predictions of the Lifshitz theory for magnetic boundary surfaces combined with the plasma model approach. It is shown that for magnetic materials the role of hypothetical patch potentials is opposite to that required for reconciliation of the data with the Drude model.

The Casimir effect [1] is of much interest due to its promising multidisciplinary applications in nanotechnology, condensed matter physics, physics of elementary particles, and in gravitation and cosmology [2,3]. Many experiments on measuring the Casimir force between boundary surfaces made of different materials separated by a vacuum gap or a liquid have been performed in the last 15 years [4–6]. It was shown that the magnitude of the Casimir force can be controlled by using different boundary materials [7,8], phase transitions [9–13], and by using the boundary surfaces structured with nanoscale corrugations [14–17].

A unified description of both the van der Waals and Casimir forces is given by the Lifshitz theory [18] in terms of the dielectric permittivity $\varepsilon(\omega)$ and magnetic permeability $\mu(\omega)$. The role of magnetic materials in the Casimir force has been studied theoretically [19–30]. The interest stems from the possibility to obtain a repulsive Casimir force for application in micromachines. Using real magnetic materials [21,25] did not validate the early results which used constant ε and μ. As $\mu(i\xi)$ can be large only at $\xi < 10^5 - 10^9$ Hz, its entire contribution to the Lifshitz formula is through the zero Matsubara frequency [27,28]. For metals, the zero-frequency term is strongly influenced by the inclusion (Drude model approach) or neglect (plasma model approach) of the relaxation properties of free electrons [4]. Thus using μ provides another parameter to study the role of the relaxation properties of free electrons in the Casimir effect. Some experiments demonstrate strong disagreement between the measured data and theoretical predictions when the relaxation properties of electrons are taken into account for metals [4,31,32] or the dc conductivity is included for dielectrics [4,12,13]. The same data are found to be consistent with theory when the relaxation properties are neglected for metals or the dc conductivity of dielectrics is disregarded. Two other experiments [33,34] are claimed to be in favor of the Drude model approach (see critical discussion in Refs. [35–38]). It was also hypothesized [39] that the effect of large

patches might bring the experimental data of Ref. [31] in agreement with the predictions of the Drude model approach (see also discussion in Ref. [32]).

In this Letter we describe the demonstration of the Casimir force between surfaces of a plate and a sphere, both coated with ferromagnetic metal Ni, performed by means of a dynamic atomic force microscope (AFM) using the frequency shift technique. The Lifshitz theory was generalized for the case of magnetic bodies in Ref. [19], but until now was not unequivocally verified experimentally. Note that measurements of the Casimir interaction between an Au-coated sphere and a Ni-coated plate [40] confirmed the influence of magnetic properties on the Casimir force under an assumption that the plasma model approach is adequate (for Au interacting with Ni the Drude model approach is not sensitive to magnetic properties and leads to almost the same results as the plasma model approach [40]). The advantage of the Ni-Ni test bodies used here is that the magnetic properties significantly affect the Casimir force when both the plasma and Drude model approaches are used leading to considerably different results [27]. Using this property, we have unequivocally confirmed that the magnetic properties influence the Casimir force in accordance with predictions of the Lifshitz theory. The agreement is excellent with the plasma model approach, and the Drude model approach is excluded by our data at a 95% confidence level. We have also excluded any possible role of patch effects on the conclusions obtained. This opens opportunities for far-ranging applications of the magnetic Casimir effect in nanotechnology including the realization of the Casimir repulsion through a vacuum gap [26–28,30].

Here we have used the same apparatus and cantilever preparation as in Refs. [32,40]. The gradient of the Casimir force was measured acting between a Ni-coated hollow glass microsphere of $R = 61.71 \pm 0.09~\mu$m radius attached to the tip of a rectangular Si cantilever and a Si plate also coated with Ni. The thicknesses of the Ni coatings were 210 ± 1 nm and 250 ± 1 nm on a sphere and a

plate, respectively. The hollow sphere leads to higher resonant frequencies and mechanical Q factors offering higher sensitivities. To promote adhesion of the Ni coating, a 10 nm layer of Cr followed by 40 nm layer of Al was done first. The coatings were performed at 10^{-6} Torr. To achieve uniformity of Ni layers, the sample was rotated during evaporation of the metals. A coating rate ≈ 3 Å/s was used. Both test bodies were cleaned using a multistep procedure to remove any attached adsorbates (both neutral and with net charge) and debris (see Ref. [32] for details). The cantilever was clamped in a specially fabricated holder and placed inside the vacuum chamber that was capable of reaching a pressure of 10^{-9}Torr by using mechanical, turbo and ion pumps. The Ni-coated plate was fixed on the top of the piezo with double sided vacuum adhesive tape. The movement of the piezo was calibrated by a fiber interferometer with 635.0 ± 0.3 nm laser source.

The dynamic measurement scheme in the frequency modulation mode, as in Refs. [32,40,41], was used. The directly measured quantity was the change of resonant frequency of the periodically driven cantilever which was detected by a phase locked loop system [42,43] (see details for our setup in Refs. [32,40]). The driving frequency was kept near the resonance frequency of the cantilever to obtain the highest signal to noise ratio. The resonance frequency was detected with an optical interferometer [43,44]. To keep the interferometric cavity length between the top of the cantilever and the end of the fiber fixed, we used a piezo above the cantilever, which was controlled by a proportional-integral-derivative feedback loop. This prevents errors in the sphere-plate separation distance a due to cantilever deflection from Casimir, $F(a)$, and electrostatic, $F_{el}(a)$, forces.

For small oscillations in the presence of an external force $F_{tot}(a) = F_{el}(a) + F(a)$, the measured frequency shift $\Delta\omega = \omega_r - \omega_0$ is expressed [32,40] as $\Delta\omega = -(\omega_0/2k)F'_{tot}(a)$. Here, ω_r is the resonance frequency in the presence of F_{tot}, ω_0 is the natural resonance frequency, k is the spring constant of the cantilever, and $a = z_{piezo} + z_0$ (z_{piezo} is the plate movement due to the piezoelectric actuator which is calibrated interferometrically and z_0 is the point of the closest approach between the two surfaces, which in our case is much larger than the separation on contact). The electric force can be expressed as $F_{el}(a) = X(a, R)(V_i - V_0)^2$, where $X(a, R)$ is the known function [3,4,32], V_i are the voltages applied to the plate, and V_0 is the residual potential difference. In terms of the measured parameters, $\Delta\omega$ takes the form

$$\Delta\omega = -\beta(V_i - V_0)^2 - CF'(a), \qquad (1)$$

where $C = \omega_0/(2k)$ and $\beta \equiv \beta(z_{piezo}, z_0, C, R) = CX'(a, R)$.

A sufficiently precise electrostatic calibration, i.e., determination of V_0, z_0, C, and β from measurements of electric forces, is possible because we use a large perfectly shaped sphere made from the liquid phase. The theoretical

electric force in the sphere-plane geometry is known exactly and the potential between a sphere and a plane can be precisely determined. For electrostatic calibrations and measurements of $\Delta\omega$, 11 different voltages in the range from -64.5 to 31.6 mV were applied to the Ni plate, while the sphere remained grounded. The plate was moved toward the sphere starting at the maximum separation of 2.3 μm and the corresponding $\Delta\omega$ was recorded at every 0.14 nm. Continuous triangular voltages at 0.01 Hz were applied to the tube piezo to move the plate toward the sphere. This set of measurements was repeated three times. The small mechanical drift 0.003 nm/s in the z_{piezo} was corrected as described in Refs. [32,40]. The parabolic dependence of $\Delta\omega$ on V_i was used to find V_0 at each separation [13]. Note that V_0 is separation independent indicating the lack of any adverse surface contaminants and the high quality of the measured data (see Fig. 1 where the best fit of V_0 to the straight line leads to a slope equal to only 1.5×10^{-5} mV/nm). The mean value of $V_0 = -17.7 \pm 1$ mV was found. The values of z_0 and C were found by a least χ^2 fitting of β in Eq. (1). The mean values are $z_0 = 221.1 \pm 0.4$ nm and $C = 52.4 \pm 0.16$ kHz m/N (the errors are indicated at a 67% confidence level). Then we obtain $\beta = (\pi\epsilon_0 CR/a^2)(1 - 2c_1a^2/R^2 - 4c_2a^3/R^3 + ...)$, where c_1 and c_2 are given in Ref. [3] and ϵ_0 is the permittivity of vacuum. The absence of calibration errors in the obtained values of z_0 and C was confirmed by their independence of the separation region used in calibration [32,40]. After the values of z_0 and C were found, the measured $\Delta\omega$ was converted into $F'_{tot}(a)$ and the absolute separation distances were determined.

Now the 33 values of $F'(a)$ at each a can be obtained from Eq. (1) by subtracting the contribution of $F'_{el}(a)$. They are shown in Fig. 2 at a from 223 to 320 nm with a step of 2 nm. The statistical properties of the data are characterized by the histogram shown in an inset to Fig. 2 at $a = 250$ nm. It is described by Gaussian distribution with the standard deviation $\sigma_{F'} = 0.92$ μN/m and mean $F' = 74.17$ μN/m. The mean values of $F'(a)$ as a function of a (with a step of 1 nm) are shown as crosses in Figs. 3(a)–3(d) where the arms of the crosses indicate the total experimental errors found at a 67% confidence level.
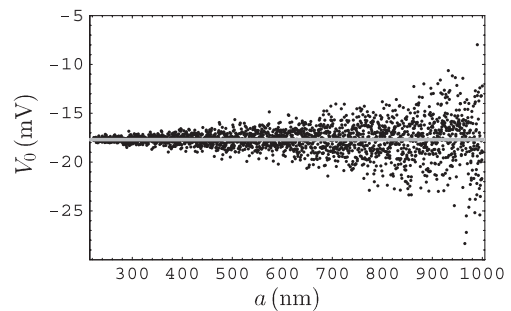

FIG. 1. The residual potential difference between a Ni-coated sphere and a Ni-coated plate as a function of separation. The mean value of V_0 is shown by the gray line.
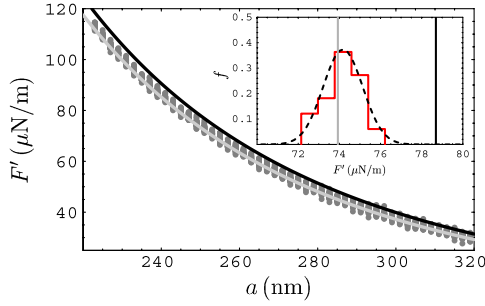
FIG. 2 (color online).   Comparison between the nonaveraged experimental data for F' (gray dots) and theory (black and gray bands computed using the Drude and plasma model approaches, respectively). The inset shows the histogram for the measured F' at $a = 250$ nm. f is the fraction of 33 data points having the values of F' in the bin indicated by the respective vertical lines. The corresponding Gaussian distribution is shown by the dashed line. The black and gray vertical lines show the theoretical predictions of the Drude and plasma model approaches.

The total errors are mostly determined by the systematic errors which are caused by the errors in calibration. Thus, the systematic errors in $F'(a)$ at $a = 223, 250, 300$, and 350 nm are equal to 1.20, 1.05, 0.89, and 0.81 μN/m (i.e., 1.1%, 1.4%, 2.4%, and 3.9% of the force gradient), respectively. These are quite sufficient to discriminate between different theoretical predictions (see below). The random error is equal to only 0.18 μN/m and does not depend on a.

The experimental data for $F'(a)$ were compared with predictions of the Lifshitz theory. The Lifshitz formula for magnetic materials [3,19–22] was adapted for sphere-plate geometry using the proximity force approximation (this leads to $< a/R$, i.e., $<0.36\%$ error at the shortest separation [45,46]) with the result

$$F'(a) = 2k_B T R \sum_{l=0}^{\infty}{}' \int_0^\infty q_l k_\perp dk_\perp \sum_\alpha \frac{r_\alpha^2}{e^{2aq_l} - r_\alpha^2}. \quad (2)$$
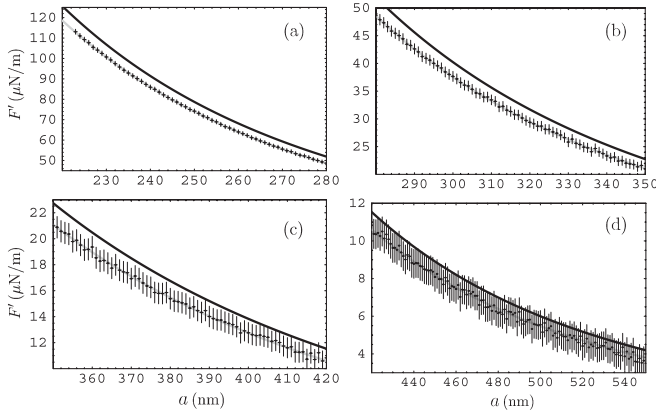

FIG. 3.   Comparison between the experimental data for F' (crosses plotted at a 67% confidence level) and theory (black and gray bands computed using the Drude and plasma model approaches, respectively).

Here, k_B is the Boltzmann constant, $T = 300$ K is the temperature at the laboratory, $q_l^2 = k_\perp^2 + \xi_l^2/c^2$, and $\xi_l = 2\pi k_B T l/\hbar$ with $l = 0, 1, 2, \ldots$ are the Matsubara frequencies. The prime multiplies the term with $l = 0$ by $1/2$ and the sum with respect to α implies a summation in the transverse electric ($\alpha = $ TE) and transverse magnetic ($\alpha = $ TM) polarizations of the electromagnetic field. The respective reflection coefficients are given by

$$r_{\rm TM} = \frac{\varepsilon_l q_l - k_l}{\varepsilon_l q_l + k_l}, \qquad r_{\rm TE} = \frac{\mu_l q_l - k_l}{\mu_l q_l + k_l}, \quad (3)$$

where $k_l^2 = k_\perp^2 + \varepsilon_l \mu_l \xi_l^2/c^2$, and $\varepsilon_l \equiv \varepsilon(i\xi_l)$, $\mu_l \equiv \mu(i\xi_l)$.

The permittivity ε_l was obtained from the optical data [47] for the complex index of refraction of Ni using the Kramers-Kronig relation. The data were extrapolated to zero frequency either by means of the Drude or the plasma models. The plasma frequency $\omega_p = 4.89$ eV and the relaxation parameter $\gamma = 0.0436$ eV have been used [47,48]. At $l = 0$ the magnetic properties of Ni were described by the static magnetic permeability $\mu_0 = 110$. For all $l \geq 1$ at $T = 300$ K, $\mu_l = 1$ because $\mu(\omega)$ rapidly falls to unity with increasing ω [27].

The theoretical force gradients $F'(a)$ were computed using Eqs. (2) and (3). The obtained values were corrected for the presence of surface roughness. The roughness profiles were investigated using an AFM and the rms roughness on the sphere and the plate was found to be $\delta_s = 1.5$ nm and $\delta_p = 1.4$ nm, respectively. At separations $a \geq 223$ nm this allows the use of the multiplicative approach [3,4,32,40]. The theoretical results are shown in Figs. 2 and 3(a)–3(d) within different separation regions by the black and gray bands (their widths are defined by the errors in the optical data) for the Drude and plasma model approaches, respectively. Note that at the separations considered the difference between the predictions of the Drude and plasma models for F' is approximately proportional to a^{-3}. As can be seen in Fig. 3, the Drude model approach is excluded by the data at a 67% confidence level over the region from 223 to 420 nm. The plasma model approach is in excellent agreement with the data. In Fig. 4 we plot the same data for F', but with the total experimental errors determined at a 95% confidence level over the region from 223 to 350 nm (in the inset the interval from 300 to 350 nm is shown on an enlarged scale). The errors at the 95% confidence level are obtained in a conservative way as the doubled errors found at the 67% confidence level [49]. As can be seen in Fig. 4, over the region from 223 to 350 nm the Drude model approach is excluded even at a higher, 95%, confidence level. For a from 420 to 1000 nm both the plasma and Drude model approaches are consistent with the data. It should be noted, however, that at large a the data are not informative with respect to the two models. Thus, at $a = 400, 550, 750$, and 1000 nm the total relative experimental error is equal to 6%, 20%, 100%, and 321%, respectively, whereas the respective differences
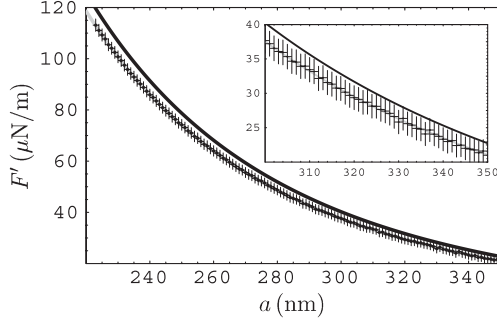
FIG. 4. Comparison between the experimental data for F' plotted at a 95% confidence level and theory (black and gray bands computed using the Drude and plasma model approaches, respectively).

between the predictions of the Drude and plasma model approaches are equal to 8.5%, 10%, 12%, and 14%.

We emphasize that according to the Lifshitz theory the magnetic properties of Ni in a Ni-Ni system significantly influence the gradient of the Casimir force in the framework of both theoretical approaches (they increase F' when the Drude model approach is used and decrease it if the plasma model approach is applied). Thus, our measurements unequivocally demonstrate the influence of magnetic properties on the Casimir force as is predicted by the Lifshitz theory combined with the plasma model approach. Of even greater importance is the fact that for two magnetic metals the Lifshitz theory predicts $F'_D > F'_p$ where the Drude and plasma model approaches are indicated by the indices D and p (see Figs. 3 and 4 where the black bands are above the gray). This is opposite to the case of two nonmagnetic metals where $F'_D < F'_p$ [31,32]. Thus, the inclusion of the effect of the patches in the calculation for two magnetic test bodies is in principle incapable of bringing the data in agreement with the Drude model approach because patches always lead to an additional attractive force. This proves that surface patches do not play any role in our experiments and confirms the model of patches [50] which leads to a negligibly small effect [4].

In this experiment both interacting bodies are magnetic and consist of many domains. Therefore it is necessary to analyze possible contribution of magnetic forces into the measurement results. This is done by considering two parallel Ni films of $L_x \times L_y = 0.9 \times 1.1$ cm^2 area and applying the general formulation of the proximity force approximation [3,51]. For films more than 150 nm thickness the magnetization of each domain is perpendicular to the film surfaces, i.e., has only the z component equal to $\pm M_s$, where $M_s = 435$ emu/cm^3 [52–54]. The magnetization of the first (1) and the second (2) films can be described by a function of two variables $M_z^{(1,2)}(x, y)$. In order to obtain the pair of infinite films described by the periodic functions, we perform the periodic continuation of $M_z^{(1,2)}(x, y)$ as odd function with the periods $2L_x$ and $2L_y$ and use the Fourier series

$$M_z^{(1,2)}(x, y) = \sum_{k=0}^{\infty} \sum_{n=0}^{\infty} M_{kn}^{(1,2)} \sin\frac{k\pi x}{L_x} \sin\frac{n\pi y}{L_y}. \quad (4)$$

Here, $M_{00}^{(1,2)} \equiv 0$ if the spontaneous magnetization is absent.

Next, using the standard formalism developed in magnetic force microscopy [55,56], one can calculate the magnetic field created by one Ni film and the magnetic force acting on the other film. Keeping in mind that the magnetic force between a pair of domains belonging to different films can be both attractive and repulsive, and that these domains have different size and are randomly arranged, the resulting magnetic force on a sphere is equal to zero under the condition that the spontaneous magnetization of at least one film is zero. This conclusion is obtained for a film of infinitely large area. Our Ni film of $L_x \times L_y$ area contains about 10^9 domains whose sizes are approximately equal to the film thickness [52] to minimize the magnetic energy. In this case a noncompensated gradient of the magnetic force is estimated to be less than 10^{-2} μN/m, i.e., a factor of 100 less than the experimental error.

To avoid the spontaneous magnetization of Ni films, we made them sufficiently thick and screened the weak environmental magnetic field in our setup. If, however, there is some nonzero spontaneous magnetization of both films, the resulting gradient of the magnetic force acting on a sphere, although nonzero, is negligibly small. This is because the magnetic field near the center of a large film does not depend on z for $z \ll L_x, L_y$ [57]. For example, even for a fully magnetized film (which is not the case for our setup) the gradient of the magnetic force acting on a sphere in the region of experimental separations is much less than 2×10^{-3} μN/m, i.e., much less than the experimental error in the measurements of $F'(a)$.

To conclude, we have experimentally demonstrated that the magnetic properties of Ni influence the Casimir interaction as predicted by the Lifshitz theory combined with the plasma model approach. The Drude model approach in application to magnetic metals is excluded at a 95% confidence level. We have also shown that any hypothetical patch potential will only exacerbate the deviation from the Drude model approach. The obtained results allow realization of the Casimir repulsion through a vacuum gap which could lead to many potential applications in nanotechnology.

[1] H. B. G. Casimir, Proc. K. Ned. Akad. Wet., Ser. B **51**, 793 (1948).

[2] K. A. Milton, *The Casimir Effect: Physical Manifestations of Zero-Point Energy* (World Scientific, Singapore, 2001).

[3] M. Bordag, G. L. Klimchitskaya, U. Mohideen, and V. M. Mostepanenko, *Advances in the Casimir Effect* (Oxford University Press, Oxford, 2009).

[4] G. L. Klimchitskaya, U. Mohideen, and V. M. Mostepanenko, Rev. Mod. Phys. **81**, 1827 (2009).

[5] G. L. Klimchitskaya, U. Mohideen, and V. M. Mostepanenko, Int. J. Mod. Phys. B **25**, 171 (2011).

[6] A. W. Rodriguez, F. Capasso, and S. G. Johnson, Nat. Photonics **5**, 211 (2011).

[7] F. Chen, G. L. Klimchitskaya, V. M. Mostepanenko, and U. Mohideen, Phys. Rev. Lett. **97**, 170402 (2006).

[8] S. de Man, K. Heeck, R. J. Wijngaarden, and D. Iannuzzi, Phys. Rev. Lett. **103**, 040402 (2009).

[9] G. Torricelli, P. J. van Zwol, O. Shpak, C. Binns, G. Palasantzas, B. J. Kooi, V. B. Svetovoy, and M. Wuttig, Phys. Rev. A **82**, 010101(R) (2010).

[10] G. Bimonte, Phys. Rev. A **78**, 062101 (2008).

[11] G. Bimonte, E. Calloni, G. Esposito, L. Milano, and L. Rosa, Phys. Rev. Lett. **94**, 180402 (2005).

[12] C.-C. Chang, A. A. Banishev, G. L. Klimchitskaya, V. M. Mostepanenko, and U. Mohideen, Phys. Rev. Lett. **107**, 090403 (2011).

[13] A. A. Banishev, C.-C. Chang, R. Castillo-Garza, G. L. Klimchitskaya, V. M. Mostepanenko, and U. Mohideen, Phys. Rev. B **85**, 045436 (2012).

[14] H. B. Chan, Y. Bao, J. Zou, R. A. Cirelli, F. Klemens, W. M. Mansfield, and C. S. Pai, Phys. Rev. Lett. **101**, 030401 (2008).

[15] Y. Bao, R. Guérout, J. Lussange, A. Lambrecht, R. A. Cirelli, F. Klemens, W. M. Mansfield, C. S. Pai, and H. B. Chan, Phys. Rev. Lett. **105**, 250402 (2010).

[16] H.-C. Chiu, G. L. Klimchitskaya, V. N. Marachevsky, V. M. Mostepanenko, and U. Mohideen, Phys. Rev. B **80**, 121402(R) (2009).

[17] H.-C. Chiu, G. L. Klimchitskaya, V. N. Marachevsky, V. M. Mostepanenko, and U. Mohideen, Phys. Rev. B **81**, 115417 (2010).

[18] E. M. Lifshitz, Zh. Eksp. Teor. Fiz. **29**, 94 (1955) [Sov. Phys. JETP **2**, 73 (1956)].

[19] P. Richmond and B. W. Ninham, J. Phys. C **4**, 1988 (1971).

[20] S. Y. Buhmann, D.-G. Welsch, and T. Kampf, Phys. Rev. A **72**, 032112 (2005).

[21] M. S. Tomaš, Phys. Lett. A **342**, 381 (2005).

[22] S. J. Rahi, T. Emig, N. Graham, R. L. Jaffe, and M. Kardar, Phys. Rev. D **80**, 085021 (2009).

[23] Yu. S. Barash and V. L. Ginzburg, Usp. Fiz. Nauk **116**, 5 (1975) [Sov. Phys. Usp. **18**, 305 (1975)].

[24] O. Kenneth, I. Klich, A. Mann, and M. Revzen, Phys. Rev. Lett. **89**, 033001 (2002).

[25] D. Iannuzzi and F. Capasso, Phys. Rev. Lett. **91**, 029101 (2003).

[26] F. S. S. Rosa, D. A. R. Dalvit, and P. W. Milonni, Phys. Rev. A **78**, 032117 (2008).

[27] B. Geyer, G. L. Klimchitskaya, and V. M. Mostepanenko, Phys. Rev. B **81**, 104101 (2010).

[28] G. L. Klimchitskaya, B. Geyer, and V. M. Mostepanenko, Int. J. Mod. Phys. A **25**, 2293 (2010).

[29] N. Inui, Phys. Rev. A **84**, 052505 (2011).

[30] N. Inui, Phys. Rev. A **86**, 022520 (2012).

[31] R. S. Decca, D. López, E. Fischbach, G. L. Klimchitskaya, D. E. Krause, and V. M. Mostepanenko, Phys. Rev. D **75**, 077101 (2007).

[32] C.-C. Chang, A. A. Banishev, R. Castillo-Garza, G. L. Klimchitskaya, V. M. Mostepanenko, and U. Mohideen, Phys. Rev. B **85**, 165443 (2012).

[33] A. O. Sushkov, W. J. Kim, D. A. R. Dalvit, and S. K. Lamoreaux, Nat. Phys. **7**, 230 (2011).

[34] D. Garcia-Sanchez, K. Y. Fong, H. Bhaskaran, S. Lamoreaux, and H. X. Tang, Phys. Rev. Lett. **109**, 027202 (2012).

[35] V. B. Bezerra, G. L. Klimchitskaya, U. Mohideen, V. M. Mostepanenko, and C. Romero, Phys. Rev. B **83**, 075417 (2011).

[36] G. L. Klimchitskaya, M. Bordag, E. Fischbach, D. E. Krause, and V. M. Mostepanenko, Int. J. Mod. Phys. A **26**, 3918 (2011).

[37] G. L. Klimchitskaya, M. Bordag, and V. M. Mostepanenko, Int. J. Mod. Phys. A **27**, 1260012 (2012).

[38] M. Bordag, G. L. Klimchitskaya, and V. M. Mostepanenko, Phys. Rev. Lett. **109**, 199701 (2012).

[39] R. O. Behunin, F. Intravaia, D. A. R. Dalvit, P. A. Maia Neto, and S. Reynaud, Phys. Rev. A **85**, 012504 (2012).

[40] A. A. Banishev, C.-C. Chang, G. L. Klimchitskaya, V. M. Mostepanenko, and U. Mohideen, Phys. Rev. B **85**, 195422 (2012).

[41] T. R. Albrecht, P. Grütter, D. Horne, and D. Rugar, J. Appl. Phys. **69**, 668 (1991).

[42] F. J. Giessibl, Rev. Mod. Phys. **75**, 949 (2003).

[43] D. Rugar, H. J. Mamin, and P. Guethner, Appl. Phys. Lett. **55**, 2588 (1989).

[44] B. C. Stipe, H. J. Mamin, T. D. Stowe, T. W. Kenny, and D. Rugar, Phys. Rev. Lett. **87**, 096801 (2001).

[45] C. D. Fosco, F. C. Lombardo, and F. D. Mazzitelli, Phys. Rev. D **84**, 105031 (2011).

[46] G. Bimonte, T. Emig, and M. Kardar, Appl. Phys. Lett. **100**, 074110 (2012).

[47] *Handbook of Optical Constants of Solids*, edited by E. D. Palik (Academic, New York, 1985).

[48] M. A. Ordal, R. J. Bell, R. W. Alexander, Jr., L. L. Long, and M. R. Querry, Appl. Opt. **24**, 4493 (1985).

[49] S. G. Rabinovich, *Measurement Errors and Uncertainties. Theory and Practice* (Springer-Verlag, New York, 2000).

[50] C. C. Speake and C. Trenkel, Phys. Rev. Lett. **90**, 160403 (2003).

[51] B. V. Derjaguin, Kolloid Z. **69**, 155 (1934).

[52] S. Hameed, P. Talagala, R. Naik, L. E. Wenger, V. M. Naik, and R. Proksch, Phys. Rev. B **64**, 184406 (2001).

[53] W. H. Kraan and M. Th. Rekveldt, J. Magn. Magn. Mater. **5**, 247 (1977).

[54] O. V. Snigirev, K. E. Andreev, A. M. Tishin, S. A. Gudoshnikov, and J. Bohr, Phys. Rev. B **55**, 14429 (1997).

[55] A. Wadas and P. Grütter, Phys. Rev. B **39**, 12013 (1989).

[56] D. Sarid, *Scanning Force Microscopy. With Application to Electric, Magnetic and Atomic Forces* (Oxford University Press, Oxford, 1994).

[57] J. J. Sáenz, N. Garcia, P. Grütter, E. Meyer, H. Heinzelmann, R. Wiesendanger, L. Rosenthaler, H. R. Hidber, and H.-J. Güntherodt, J. Appl. Phys. **62**, 4293 (1987).